Periodic Trends and Fluxionality Effects on Transition Metal Catalyzed Sulfoxidation

Diego Garay-Ruiz, Cristiano Zonta,* Silvia Lovat, Fátima Sanz Azcona, Joan González-Fabra, Carles Bo,* and Giulia Licini*

Read Online

ACCESS | Metrics & More | Article Recommendations | Supporting Information

ABSTRACT: Despite the extended interest in d^0 metal complexes as catalysts for peroxide activation and eventual oxygen transfer processes, there are still gaps in the understanding of how they proceed at the microscopic level. Herein, we have considered sulfide oxidation with cumyl hydroperoxide as a test system, performing the reaction with a series of eight different amino-triphenolate d^0 metal complexes: Ti(IV), Zr(IV), Hf(IV), V(V), Nb(V), Ta(V), Mo(VI), and W(VI). The reactivity and selectivity of the catalytic systems, as well as the effect of a strong Lewis base (dimethylhexyl-N-oxide), have been determined experimentally, correlating kinetic values with Sanderson electronegativity values. Theoretical calculations of the catalytic cycles have been performed to have a clearer description of the role of the reactive peroxo species. Combining experimental results and DFT predictions, we propose suitable mechanisms for all eight metal aminotriphenolates, rationalizing the expected periodic trends, while also unveiling the unique reaction pathways available to highly flexible vanadium complexes.
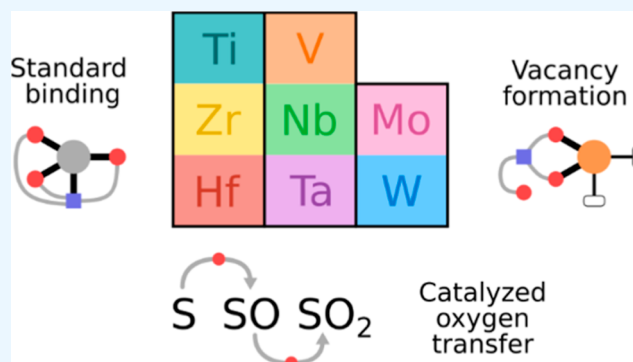
INTRODUCTION

The possibility to activate peroxides with the help of metal catalysts has an important relevance in biochemical and artificial processes and it expands applications in industrial productions.[1−3] The activation of the peroxides by metals can follow a radical pathway, in which the metal changes its oxidation state along the course of the reaction, or an electrostatic activation, in which the metal activates the peroxide on in virtue of its Lewis acidic properties without changing its oxidation state. While the first method of activation is more common to late transition metals (e.g., iron, manganese, or copper),[4] the second pathway is more common in d^0 early transition metals. It should be also noticed that d^0 metals (e.g., Ti and Zr) can also activate hydrogen peroxide homolytically without the change of the metal oxidation state.[5,6] Among the possible d^0 metals available, some of them have been used more extensively and effectively than others. The classical example is the sharpless stereo-selective allylic alcohol oxidation carried out by d^0 titanium-(IV) tartrate and alkyl hydroperoxides.[7] However, other d^0 metals have also been used: vanadium(V) for sulfoxidations, epoxidation, and haloperoxidation reactions;[8] and Mo(VI) have been extensively used in epoxidation reactions and in the Halcon process.[9] Other d^0 metals, such as Ta(V),[10] Zr-(IV),[11−13] and Nb(V)[10,14] have been used in oxidation reactions but less extensively. In this context, polyoxometalate

derivatives also arise as another relevant class of d^0-metal-based systems capable of peroxide activation.[15−19]

Even if the mechanism of oxygen transfer has been, and continues to be, a controversial subject, it is becoming widely accepted that it involves a "Sharpless type" pathway. In this, the active species is an η^2 coordinated alkyl (or hydro) peroxo complex and the nucleophilic attack of the substrate to the electrophilic peroxo oxygen is along the antibonding σ^* (O_1-O_2). However, despite the large interest in the subject, few studies have compared the reactivities of different d^0 metals in order to dissect "periodic" trends. Among these studies, the contribution of the group of Rosch must be noticed, which studied the reactivity of d^0 peroxo complexes toward epoxidation.[20] What emerges from these studies is that the activity of the peroxo complexes is related to three factors: the strength of the $M-O_1$ and O_1-O_2 interactions, the charges in the O_2 oxygen atoms, and the interaction between the unoccupied peroxo σ^* orbital and the HOMO of the substrate. Very interestingly, in the study where they were comparing
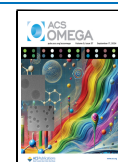
Table 1. Kinetic Data for the Oxidation of S with CHP Catalyzed by Metal Aminotriphenolate Complexes[a]

M	L₁	L₂
Ti	-OiPr	/
Zr	-OtBu	/
Hf	-OtBu	/
V	=O	/
Nb	OEt	OEt
Ta	OnBu	OnBu
Mo	=O	Cl
W	=O	Cl

cat	oxygen mass balance (%)	time (h)	conv. S (%)[b]	yield SO (%)[b]	yield SO₂ (%)[b]	SO/SO₂	k_1[c]	k_2[c]	k_1/k_2
Ti	>99	40	84	67	17	80:20	1583	380	4.2
Ti NO	97	72	80	62	18	78:22	865	315	2.7
Zr	>99	10	58	15	43	26:74	5188	25,821	0.20
Zr NO	93	100	59	25	34	42:58	690	322	2.1
Hf	>99	3	59	17	42	30:70	8030	31,200	0.3
Hf NO	99	700	62	25	37	40:60	290	171	1.7
V	>99	35	96	91	5	96:4	820	2	410
V NO	>99	1	90	80	10	90:10	46,189	4450	10
Nb	>99	550	94	87	7	92:8	442	49	9
Nb NO	90	980	88	85	3	97:3	85	8	11
Ta	>99	300	80	59	21	74:26	404	132	3
Ta NO	88	2400	80	72	8	90:10	38	5	8
Mo	>99	360	97	94	3	98:2	40	1	40
Mo NO	>99	300	92	83	9	90:10	147	7	21
W	>99	300	99	98	1	99:1	97	4	24
W NO	99	300	90	81	9	90:10	42	6	7

[a]Reaction conditions: 25 °C, $[S]_0 = [CHP]_0 = 0.1$ M, $[M] = 0.001$ M. [b]Sulfide conversion, SO, and SO₂ yields determined by ^{1}H NMR analysis on the crude reaction mixture after complete oxidant consumption (iodometric test). [c]Determined using nonlinear fitting of a pseudo first-order equation of the first 20% of the reaction for SO and full interpolation for the SO₂ (in mol$^{-3}\cdot$h^{-1}).

Cr(VI), Mo(VI), and W(VI), it is clear that the ionic radius was directly linked to the electronic charge on the reactive oxygen. The smaller the radius, the lower the charge at the reactive oxygen. However, because the oxidation of olefins limits the study to few metals, we decided to start a systematic study using sulfoxidation as an experimental tool to compare the reactivity among different d⁰ metal complexes. Sulfoxidation reaction gives several potential advantages, one being the capability of most of the d⁰ peroxo-metal complexes to oxidize sulfides, giving rise to a wider analysis along the periodic table. Moreover, it is also possible to take advantage of the second oxidation step to sulfone which can give more information on the reactive peroxo metal complex. The study has been planned by preparing eight d⁰ aminotri-t-butyl-phenolate metal complexes, namely, Ti(IV), Zr(IV), Hf(IV), V(V), Nb(V), Ta(V), Mo(VI), and W(VI) and testing their activity in sulfoxidation reactions. This ligand has been chosen because it has shown for some of these complexes a well-defined coordination geometry and for the capability, given by the ortho t-butyl substituents, to form stable and monomeric complexes in solution.[21]

In addition to this systematic study of the reactivity of different metal complexes, we have also considered the effect of an external Lewis base (LB) on the reactivity. In fact, in some of our studies we have noticed that d⁰ metal complexes have the inclination to expand their coordination sphere in the presence of external LBs, showcasing sensible differences on the reactivity, stability and selectivity in oxygen transfer reactions.[22]

Herein, we report a detailed study on the synthesis of eight aminotriphenolate complexes and on their catalytic activity in sulfoxidation of methyl-p-tolyl sulfide (**S**) in the presence and absence of a strong LB, dimethylhexyl-N-oxide (**NO**). In this context, the well-known sulfoxidation reaction provides an ideal test playground to assess the similarities and fundamental differences on the catalytic pathways undergone by the eight target complexes as well as the correlation of the reactivities and selectivities with descriptors such as Sanderson electronegativity (SE). To this end, we combined experimental results and computational studies in order to get the most complete picture of the underlying mechanisms.

■ RESULTS AND DISCUSSION

Synthesis of the Complexes. Triphenolamine ligand **1** has been prepared with a synthetic strategy developed in our group, which is based on a 3-fold reductive amination of the corresponding substituted salicylic aldehyde.[23] **Ti**,[24] **Zr**, **Hf**, **V**,[25] **Nb**, and **Ta** metal complexes were obtained by mixing the ligand **1** with an equimolar amount of the alkoxide salts in CDCl₃ under nitrogen atmosphere. **Mo** was prepared using a methodology developed by Lehtonen for similar ligands,[26] which uses MoO₂Cl₂ as a metal source.[27] Correspondingly, WOCl₄ was employed for **W** preparation.[28] The formation of the complexes was followed by ^{1}H NMR spectroscopy, and different reaction times were observed for the complete formation of the complexes. For all of the alkoxide exchange reactions, quantitative conversions were obtained, as shown by the ^{1}H NMR of the crude of the reaction. Coordination geometry of the final complexes was established by evaluating
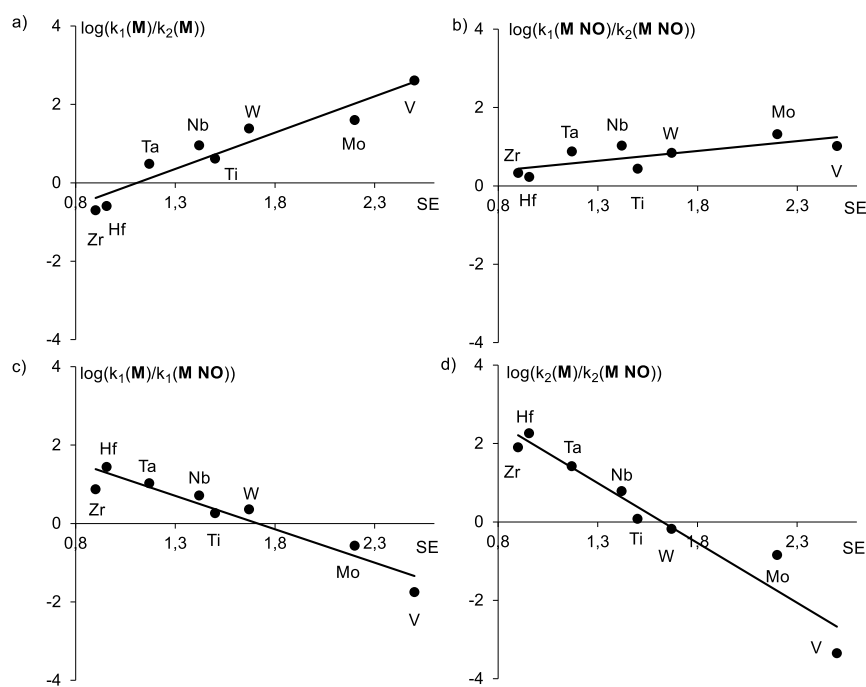
Figure 1. Plot of the relative reactivities vs the metal SE values. (a) Ratio between the rate constants of the first and second oxidation obtained using the catalyst M $[k_1 (M)/k_2 (M)]$. (b) Ratio between the rate constants of the first and second oxidation of the complex M in the presence of LB NO (5 equiv) $[k_1 (M\ NO)/k_2 (M\ NO)]$. (c) Ratio between the first oxidation rate constants of the complex M without and with the LB NO $[k_1 (M)/k_1 (M\ NO)]$. (d) Ratio between the second oxidation rate constants of the complex M without and with the LB NO $[k_2 (M)/k_2 (M\ NO)]$.

the symmetry displayed by benzylic protons in the ^1H NMR spectra (Figure S1). In C_3 symmetric systems, such as **Ti**, the complex is formed as a racemic mixture, which results from the helical wrapping of the ligand around the metal ion. The chirality of the complexes is reflected on the diastereotopicity of the benzylic methylene protons, which translates in two doublets at 3.94 and 2.89 ppm. A couple of doublets are observed also for **V** (3.77 ppm bs and 2.90 ppm bs), indicating the formation of C_3 symmetric systems and thus a trigonal bipyramidal coordination geometry. When the racemization is faster than the NMR time scale, the benzylic protons average and they result in a broad singlet. This is the case of **Zr** (3.48 ppm bs) and **Hf** (3.51 ppm, bs). In the case of octahedral arrangement, as **Mo** and **W**, in solution, the complex is C_S symmetric, and as a result, three signals are observed. This is also the case for **Nb** and **Ta**. Moreover, in all the ^1H NMR spectra, it is possible to notice the presence of the free alcohols, with the correct stoichiometric ratio, and, if present and ^1H NMR-active, the remaining ligands. Complexes have also been characterized using ESI-MS.

Catalytic Activity. Previous studies on the catalytic activity toward sulfoxidation of **Ti**, **V**, and **Mo** complexes have shown that these three catalysts perform well in terms of reactivity with alkyl peroxide or hydrogen peroxide.[24,25,27] Moreover, they can also transfer oxygen quantitatively at very low catalyst loadings. This feature is given by the high stability conferred by the polydentate ligand and its capability to inhibit the formation of multimeric species.

Standard reaction conditions for these catalysts were a concentration of 0.1 M of the substrate and of the oxidant and 0.001 M concentration of the catalyst. For this reason, we have decided to test the catalytic activity for sulfoxidation of methyl-*p*-tolyl sulfide **S** under the same conditions for all the

complexes. Every catalytic test was performed in the presence and in the absence of a strong LB, namely, dimethylhexyl-*N*-oxide **NO**, at a concentration of 0.005 M, which corresponds to five times the concentration of the catalysts. This concentration has been found to saturatively coordinate **V** complexes. The results of all the catalytic tests are shown in Table 1; this comprehends oxygen mass balance, conversion and yields of the reaction, and final SO/SO_2 ratio. Cumyl hydroperoxide (**CHP**) has been used as an oxidant due to the possible low stability of some complexes with aqueous solutions. Initial rates were also calculated for all the reaction for the first and second oxidation step.

All of the complexes have the capability to transfer oxygen from **CHP** to the thioether **S**. For most of the complexes, the transfer is quantitative. The lowest yields are associated to complexes that, in these experimental conditions, require long experimental time for completion. This could be thus explained with a possible degradation of the catalyst. From the experimental data, it has been possible to extrapolate kinetic constants for the first oxidation process from the sulfide **S** to the sulfoxide **SO** (k_1) and for the second oxidation process (k_2, Table 1). This has been calculated by nonlinear fitting of a first-order equation of the first 20% of the reaction. This was in order to have the minimal effect of the degradation of the complex and to avoid the effect, already shown by our previous work, which can have the coordination of formed sulfoxide to the reactivity of the metal complex. Experimental kinetic values are not straightforward to interpret. However, it is possible to note that more acidic metal complexes, such as **V** and **Mo**, have the tendency to form exclusively the sulfoxide, and on the other hand, more basic metals tend to favor the second oxidation process. These results have been compared using the SE values for metals.

Reactivity Comparison: Sanderson Electronegativity Values. SE values allow to have a parameter indicating the acidity−basicity of the metals.[29−33] These are based on the principle that the ability of an atom or ion to attract electrons to itself depends upon the effective nuclear charge felt by the outermost electrons. In the first approximation, they are in straight correlation among the ratio between the formal oxidation state over the ionic radius. However, it is not possible to directly correlate the reactivity and selectivity of the different metal complexes with these electronegativity parameters.

Too many factors contribute to the observed properties of the complex. In each complex, the observed reactivity values, apart from the characteristic of the metal peroxo complex, depend on many other parameters, which can be summarized as the geometry adopted by the complex, the energy requested for coordination of the alkyl peroxide, or the steric factors governing the approach of the reacting molecules to the reactive alkylperoxo complex. To remove these different factors, consideration of the activity of the peroxo complex has been carried out by comparing relative ratios of the same metal complex. More in detail, we are not comparing the reactivity of the different catalysts, but we are comparing the relative reactivities and in particular; - the ratio between the rate constant of the first oxidation and the second of the free complex (k_1 (**M**)/k_2 (**M**)),

- the ratio between the rate constant of the first oxidation and the second of the complex when the LB **NO** is present (k_1 (**M NO**)/k_2 (**M NO**)),
- the ratio between the first oxidation rate constants of the complex free and with the LB (k_1 (**M**)/k_1 (**M NO**)),
- the ratio between the second oxidation rate constants of the complex free and with the LB (k_2 (**M**)/k_2 (**M NO**)).

The correlation between the rate of the corresponding rate constant with SE value is shown in Figure 1. In the plot of Figure 1a, it is possible to note a straight correlation among the ratio of the first and the second oxidation and the SE value. This supports the fact that acid metals have the tendency to favor the first oxidation in favor of the second and vice versa for the more basic elements.

This translates into the capability of metals such as vanadium and molybdenum to create more electrophilic oxygen atoms by virtue of the capability of these metals to give the small charge separation in the M−O bond. On the other hand, a smaller radius such as in **Zr** is associated to a less pronounced electrophilic character. The preference for the first oxidation over the second is still present when we introduce LB **NO** (Figure 1b). In this case, the trend is similar but the metals display a less marked difference among them. In the absence of LB, the k_1 over k_2 range was varying from 0.2 to 410, and the addition of the LB reduced this range from 1.7 to 21. Acidic metals decrease their preference toward the first oxidation step, and in a reverse mode, more basic metals have the tendence to decrease their preference toward the second oxidation step. This tendency is also reflected when we make a direct comparison of the first oxidation with and without the LB (Figure 1c). In this case, while for acidic metals the introduction of the LB results in an increased reactivity for the first oxidation step, in the case of more basic metals, there is a strong decrement in the reactivity. Similar considerations can be drawn for the analysis of the second oxidation with and without the LB (Figure 1d).

Computational Study. The wide variety of behaviors exhibited by the different d[0] metal aminotriphenolate complexes prompted us to carry out a detailed computational mechanistic investigation. In this study, we focused on the rationalization of periodic trends (in-group or across different groups) and on the effect of the LB additive employed experimentally, which has a strong impact on both the selectivity and catalytic activity. All calculations were carried out with the PBE-D3 functional, including Perdew−Burke−Ernzerhof correlation/exchange[34,35] and Grimme's D3 dispersion[36] and a TZ2P basis set, regarding ZORA[37−39] relativistic corrections and the COSMO[40] solvent model for chloroform, in ADF 2016.1.[41] The reported Gibbs free energies (except if otherwise stated) include entropic corrections from Martin et al.[42] at the working temperature (298.15 K) and considering the density of chloroform (1.49 g/mL). To reduce the computational cost, we employed a simplified model of the catalytic system, with methyl-substituted aminotriphenolate, SMe₂, as a substrate, and HOOH as the entering peroxide. For the same reason, the dimethylhexyl-*N*-oxide additive was modeled as trimethyl-*N*-oxide. Regarding the active species for oxygen transfer, we considered hydroperoxo complexes (M-OOH) for all eight metal complexes, following the most common convention in the literature.[43−48]

The structures in Figure 2 correspond to catalyst precursors, bearing methoxy (**Ti**, **Zr**, **Hf**, **Nb**, and **Ta**), oxo (**V**), and oxo
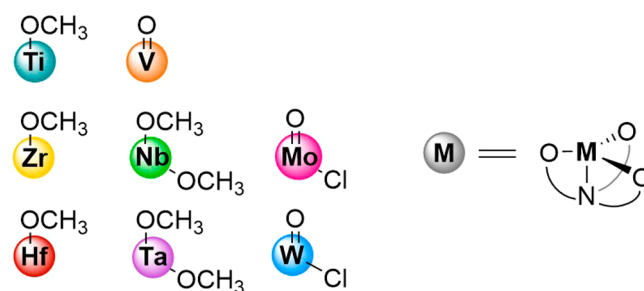

Figure 2. Substitution patterns for the eight metal catalysts under study.

and Cl (**Mo**, **W**) groups. The actual catalytic species will only be formed after a first sulfoxidation cycle, as the −OH group coming from the peroxide replaces the initial −OCH₃ or −Cl groups. For the case of **V**, this activation involves, instead, the protonation of the noninnocent aminotriphenolate ligand, as we will detail in further sections. We first studied the sulfoxide-forming catalyst activation processes for all eight metal complexes in Figure 3, obtaining a measurement of the catalytic activity of each metal that can be compared with and across groups. Furthermore, group 4 (**Ti**, **Zr**, and **Hf**) and group 5 (**V**, **Nb**, and **Ta**) metals were the subject of more detailed investigations, unraveling the respective full catalytic cycles.

Catalyst Activation. The study of the activation stage already provides relevant insights into the behavior of the overall complex. Thus, the trends observed for the experimental rate constants will be compared to the trends in the barriers for the processes in Table 2. The computed barriers effectively follow, at least qualitatively, the observed kinetic trend: group 4 metals are the fastest, in the order **Hf** > **Zr** ≫ **Ti**. Group 5 metals are slower than the ones from group 4, with **V** > **Nb** = **Ta**. Finally, in group 6, **Mo** and **W** show very
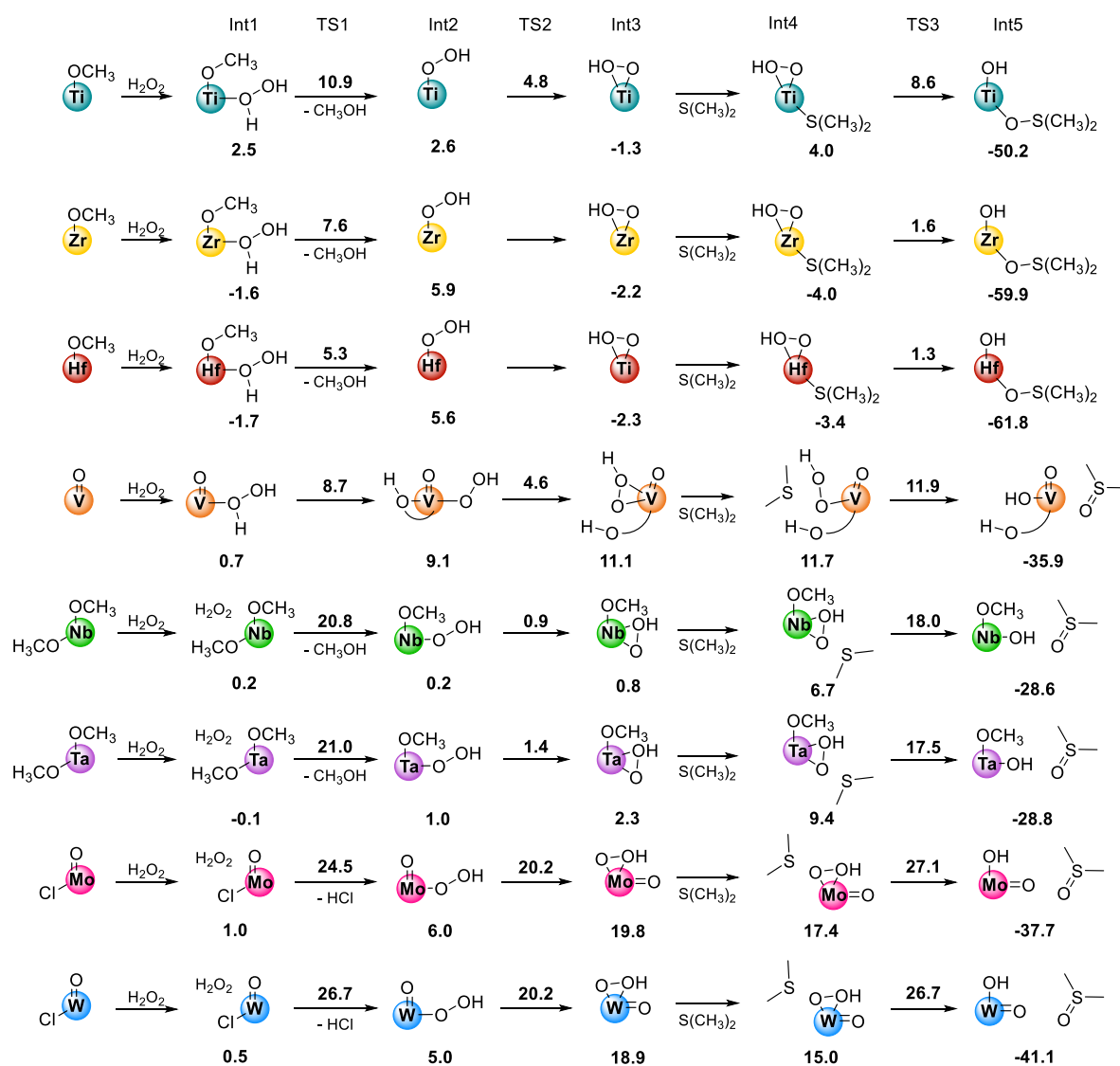
Figure 3. Catalyst activation processes for the eight studied metals. In cases where several activation pathways can occur, only the most favored one is reported (e.g., vanadium). Gibbs free energies including Martin entropic corrections, in kcal·mol^{-1}.

Table 2. Free Energy Barriers (Including Martin Entropic Corrections) in kcal·mol^{-1} and Experimental Kinetic Constants for SO Formation in the Studied Metals with and without an LB Additive[a]

	ΔG/kcal mol^{-1}	k_1 (M)/mol^{-3} h^{-1}	k_1·(M NO)/mol^{-3} h^{-1}
Ti	10.9	1583	865
Zr	9.2	5188	690
Hf	7.0	8030	290
V*	14.6	820	46189
Nb	21.0	442	85
Ta	20.8	404	38
Mo	27.1	40	147
W	26.7	97	42

[a]Entries in gray have proton transfer as the rate-determining step and non-shaded cells, S−O bond formation.

poor catalytic activity. From these preliminary results, we focused on groups 4 and 5, containing the most efficient catalysts and showing additional trends of interest (selectivity switch from sulfoxide to sulfone along group 4, unexpected reactivity boost in the presence of LB for **V**).

In the case of the group 4 metals, experimental results showed a clear switch in selectivity when going down along the group: **Ti** favors the first oxidation, leading to sulfoxide, while **Zr** and **Hf** are much faster for the second oxidation, forming sulfone. We recently reported[49] the mechanistic details for both **Ti** and **Hf**, as part of a deeper study on the changes in the binding mode of the sulfide across the group. The behavior of **Zr**, missing from that previous study, is analogous to that of **Hf**, as both have similar sizes and have the same coordination patterns. The catalytic cycles for the three metals (with the current model system using HOOH as the peroxide) are reported in the Supporting Information for completeness.

For the group 5 metals, high selectivity through first oxidation has been found for all cases, which has been also reported by Hill and co-workers in the case of **V**.[50] However, the most striking feature along the group is the anomalous
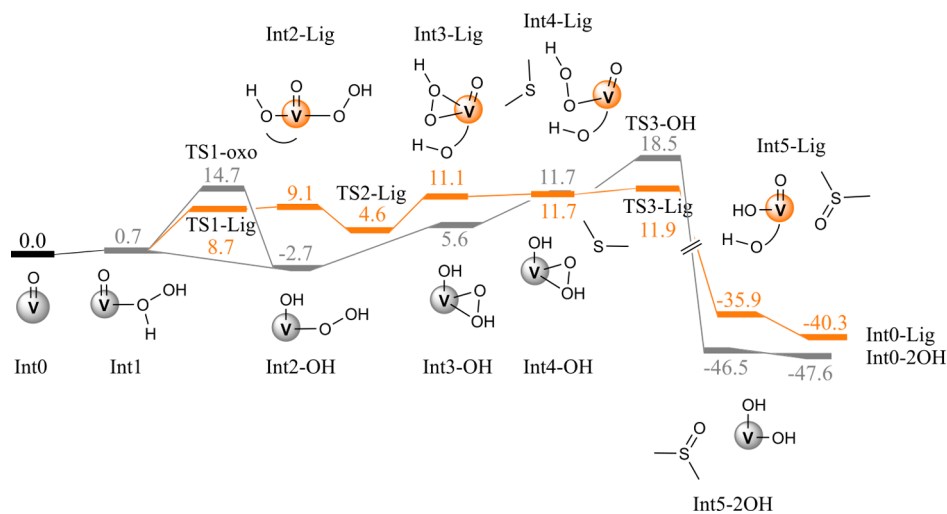
Figure 4. Activation routes for the V catalyst, including oxo group reduction (gray trace) and ligand protonation (orange trace). Martin-corrected Gibbs free energies in kcal·mol^{-1}.

behavior of the **V** catalyst when a *N*-oxide is present in the medium. This additive is a strong LB, which promptly binds to the Lewis acid metal centers. In most of the tested complexes, including the other group 5 metals **Nb** and **Ta**, the LB strongly inhibits the activity of the catalyst. This can be associated with the formation of stable off-cycle adducts that lower the resting state of the corresponding catalytic cycles, increasing the net barriers. In sheer contrast, the activity of the **V + LB** system is deeply enhanced, becoming the most active catalyst of the set. To properly explain this feature, we investigated the complete sulfoxidation mechanisms for **V**, **Nb**, and **Ta**, as detailed in the following sections. Finally, with regard to the group 6 metals, experimental results showed **Mo** to be the metal center with the poorest catalytic performance of the set. This is in good agreement with the catalyst activation route in Table 2, with a 27.1 kcal·mol^{-1} barrier that is substantially larger than any of the activation energies reported for metals in groups 4 and 5. Tungsten, as expected, has a very similar behavior with a 26.7 kcal·mol^{-1} barrier. Due to the poor activity of the two complexes, no deeper characterization of the complete catalytic cycles was attempted in this case.

Catalytic Cycles for Group 5 Metals. While the differences along the catalytic complexes in group 4 depended only on the nature and size of the metal center, the analysis of the M^{5+} cations must consider the changes in substitution patterns along the group. **Nb** and **Ta** bear two methoxy substituents together with the aminotriphenolate ligand, allowing for a mechanism via protonation/alcohol release as metals in group 4. As the **V** catalytic precursor is a 5-coordinated bipyramid trigonal structure with a single oxo group instead of the two methoxides, this scheme cannot take place at all.

As shown in Figure 4, a possible manifold involves the protonation of the oxo substituent (gray route), which is formally reduced to a hydroxo moiety, thus eventually generating a V-dihydroxo active species. However, ligand involvement enables an alternative pathway through the protonation of any of its equatorial O atom (orange route). This approach produces a V-oxoperoxo intermediate, from which the oxidation of sulfide can readily take place. The ligand protonation scheme allows the complex to maintain the V═O group, a very common and stable motif in the

coordination chemistry of vanadium, which consequently shows a lower activation energy than the oxo-protonation path.

Nevertheless, both oxo-protonation and ligand-protonation routes suppose major changes in the structure of the metal complex: the catalytically active species would be **Int0-2OH**, a dihydroxo complex, and **Int0-Lig**, an oxo−hydroxo complex with a decoordinated phenol in the ligand. Also, in contrast with the routes for the other studied metals, no subproduct is released in any way in this step. Because of this, the barriers for catalyst activation in **V** are not a valid estimation of the catalytic activity: it is then necessary to explore the mechanisms starting from the two possible active complexes. Moreover, to put everything in context, we also characterized the more straightforward mechanisms for **Nb** and **Ta**, so we had a proper reactivity comparison along the group (Figure 5). The rate-determining step for **Nb** and **Ta** is the proton transfer
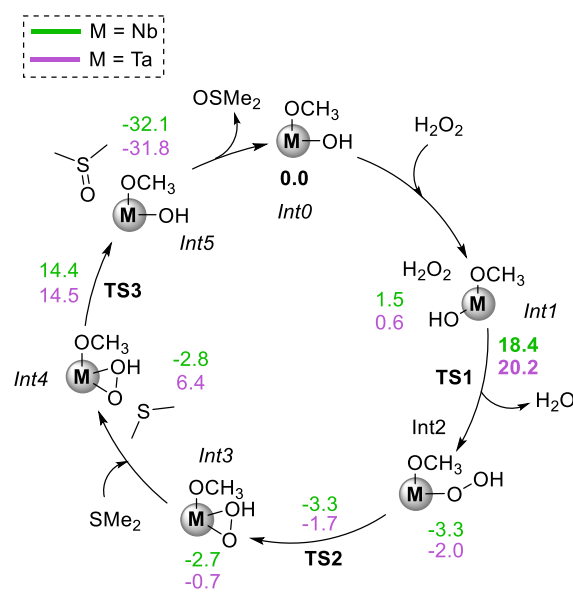

Figure 5. Catalytic cycle for sulfide oxidation for Nb and Ta catalysts, starting from the hydroxy−methoxy complexes formed after activation. Gibbs free energies including Martin entropic corrections, in kcal·mol^{-1}.

stage, leading to water release (**TS1**), with barriers of 18.4 and 20.2 kcal·mol^{-1}: while the difference between the two is larger than expected, with the two complexes having very similar experimental kinetic constants; the qualitative trend is maintained.

The oxo-protonation manifold for vanadium implies that an initial proton transfer/water release step (from **Int0-2OH**) does already show a barrier of 21.0 kcal·mol^{-1}. This would imply a slower reaction than with **Nb** or **Ta** against experimental observations. In contrast, the ligand-protonation scheme (Figure 6), also having proton transfer as its rate-determining step, has a barrier of only 18.0 kcal·mol^{-1}, which recovers the expected trend.
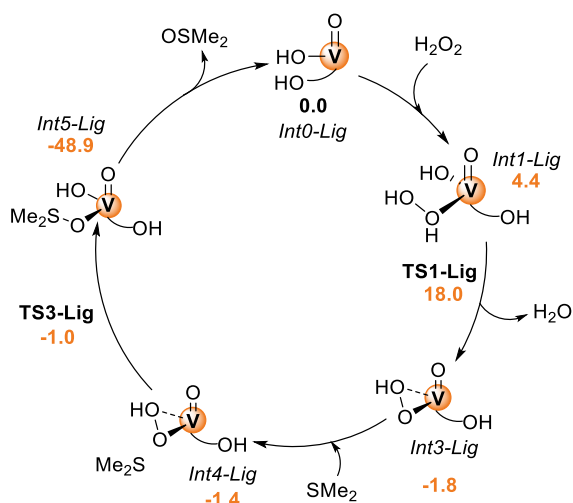
Figure 6. Catalytic cycle for the protonated-ligand sulfoxidation route in **V**, starting from the oxo–hydroxo complex Int0-Lig. Gibbs free energies including Martin entropic corrections, in kcal·mol^{-1}.

Once the hydrogen transfer has occurred, the final S–O bond formation from **Int4-Lig** is extremely facile (through the low-lying transition state **TS3-Lig** at −1.0 kcal·mol^{-1}), completing the catalytic cycle. Throughout this whole pathway, there is a remarkable evolution in the coordination number of **V** along the cycle, going from tetrahedral **Int0-Lig** to octahedral **Int5-Lig**. Once the initial oxygen atom in the aminotriphenolate moiety is protonated, it detaches from the metal center. After this first decoordination event, the conformational flexibility of the complex allows a second decoordination to take place, with the N atom being able to leave the coordination sphere of vanadium with minor penalties. Thus, the ligand goes from its usual 4-coordinated binding mode to a 2-coordinated one, allowing for the formation of formally tetrahedral complexes such as **Int0-Lig**. From there, the nitrogen atom freely binds and detaches from vanadium to allocate other groups along the mechanism: the corresponding N–V distances and coordination geometries are shown in Table 3.

For selected structures (**TS1-Lig**, **Int3-Lig**, and **TS3-Lig**), tridimensional structures and representations of the coordination environment of V are shown in Figure 7.

Despite the apparent undercoordination of tetrahedral-like structures such as **Int0-Lig** or **TS3-Lig**, their energies are very much in line with the more common trigonal bipyramid or octahedral motifs. The combination of the flexibility of the ligand, especially once it has detached the protonated arm, and

Table 3. Evolution of Nitrogen–Vanadium Bonding Along the Ligand Protonation-Based Mechanism, Including N–V Distance (in Å), Geometry of the Metal, and Presence of a BCP between N and V

complex	N–V/Å	geom.	BCP N–V?
Int0-Lig	3.33	tetrahedral	No
Int1-Lig	2.95	octahedral	Yes
TS1-Lig	3.36	trig. bipyr.	No
Int3-Lig[a]	2.82	trig. bipyr.	Yes
Int4-Lig[a]	2.97	trig. bipyr.	Yes
TS3-Lig	3.24	tetrahedral	No
Int5-Lig	2.91	octahedral	Yes

[a]Structures with chelated hydroperoxo group. Regarding coordination number, the hydroperoxo is considered to occupy a single vacant.

the capability of V(V) for stabilizing different coordination numbers results in noteworthy fluxionality, enabling the mechanism in Figure 6. The stabilization of the hydroperoxo group that is formed after proton transfer can be rationalized through the same explanation: separating the N atom enables the system to reduce the steric crowding. Thus, the intermediates **Int3-Lig** and **Int4-Lig**, as well as the key transition state **TS3-Lig**, are highly stabilized.

The main question left to answer for vanadium is the reason behind the deep enhancement of the catalytic activity in the presence of an *N*-oxide in the medium. As shown in Table 1, **V** shows a more than 50-fold increase in its sulfoxidation rate constant, from 820 to 46,189 mol^{-3} h^{-1} when the base is in the medium. In contrast, **Nb** and **Ta**, like most of the other metals, are strongly inhibited, with 5-fold and 10-fold decreases, respectively. In fact, when the trimethyl-*N*-oxide binds to **V**, the complex is stabilized, just like for the other metals.

However, the fluxionality of the partially protonated structure allows the complex to accommodate the LB together with the reactants, as the tetrahedral-like structure of **Int0-Lig** provides two vacant sites on the metal. As shown in Figure 8, one of these sites is occupied by the *N*-oxide, but the spot left by nitrogen gives room for the peroxide to approach the complex at the same time as the LB. Just like for the initial mechanism, we considered the extent of N–V bonding across the complexes in the current scheme (Table 4), regarding the activation stage leading to the in-cycle complex **Int0-LB-N**.

The extensive fluxionality of vanadium complexes is showcased again, evolving from tetrahedral to octahedral and to axial–equatorial exchanging trigonal bipyramids. Proper nitrogen–vanadium coordination is only present on **Int0-LB**, which shows the smallest N–V distance and a bond critical point (BCP) from Bader analysis. Neither of the other complexes show N–V bonding at all, with distances going beyond 3 Å and no BCPs.

Coming back to the discussion of catalytic activity, once **Int0-LB-N** is formed, the *N*-oxide contributes to the sulfoxidation process instead of hindering it, as the additional stabilization that it confers to the complex lowers the energies of the upcoming intermediates and transition states. Geometries and coordination environments of selected structures throughout this part of the cycle are depicted in Figure 9. Looking at the main bottleneck of the catalytic cycle, the H-transfer, we find that the peroxide can be accommodated by interacting with the perpendicular equatorial hydroxy group, which captures the proton from the substrate and is then released as water. Thus, the H-transfer stage happens with a
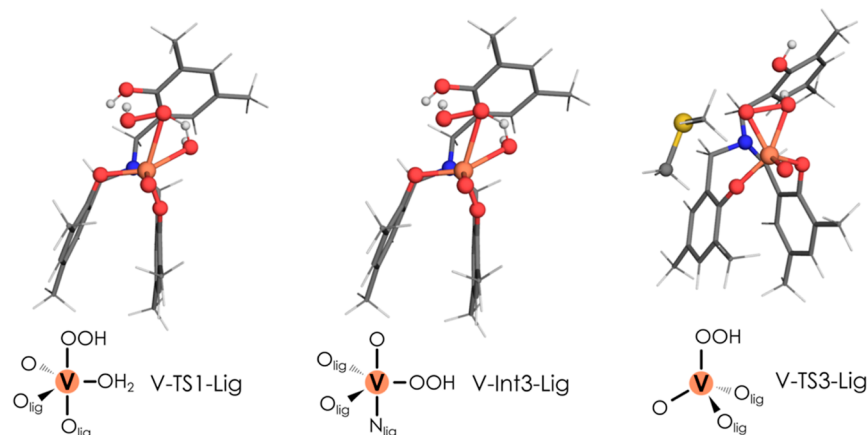
Figure 7. Selected tridimensional structures for V-mediated sulfoxidation, including proton transfer TS (V-TS1-Lig), hydroperoxo intermediate (V-Int3-Lig), and sulfoxidation TS (V-TS3-Lig). The immediate coordination environment of V(V) is represented schematically next to the corresponding label.
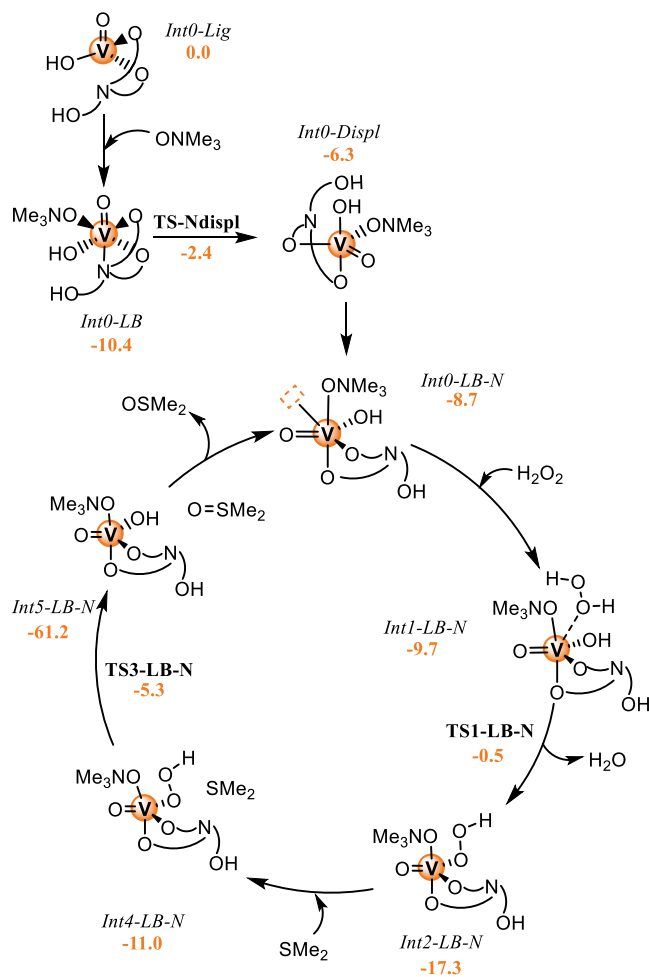

Figure 8. Catalytic cycle for V + LB system, involving N decoordination. Gibbs free energies including Martin entropic corrections, in kcal·mol^{-1}.

Table 4. Selected Geometric Parameters for Complexes Formed in the Presence of N-Oxide, Including N−V Distance, N−V−O Angle for the Equatorial Plane in the Ligand, and Geometry of the Metal Center

complex	N−V/Å	N−V−O$_{eq}$/°	geom
Int0-Lig	3.33	106.7	tetrahedral
Int0-LB	2.71	90-5	octahedral
TS-Ndispl	3.43	89.2	trig. bipyr. (OH ax.)
Int0-Displ	3.70	87.6	trig. bipyr. (OH ax.)
Int0-LB-N	3.63	93.0	trig. bipyr. (LB ax.)

overall effect is a net decrease of the reaction barrier (6.0 kcal·mol^{-1}).

This qualitatively explains the observed enhancement of activity, while also being very consistent with the features observed in the nonaccelerated mechanism. It is remarkable that all intermediates in the final cycle maintain a trigonal bipyramid coordination: neither HOOH (**Int1-LB-N**), SMe$_2$ (**Int4-LB-N**), nor the sulfoxide (**Int5-LB-N**) coordinate directly to the metal center, with the corresponding octahedral intermediate complexes not being stable minima in the potential energy surface. These findings are in line with the convoluted inner/outer sphere behavior we already reported[49] for the Ti and Hf complexes.

Apart from the proposed catalytic cycle, several alternative structures for V + LB + HOOH reactive complexes were explored, as shown in Figure 10. We found stable complexes where either the peroxide (**Int1A**, **Int1B**, and **Int1C**) or even the LB (**Int1D**) are not covalently bound to V, but held together by H-bond-based interactions between the protonated phenol group in the ligand, the hydroxy group, the N-oxide, and the hydrogen peroxide. Octahedral structures are the most common, but other situations, such as the very stable **Int3D**, tetrahedral-like, or **Int1B**, between the octahedral and the trigonal bipyramid limits, still arise. While the pathway in Figure 8 remains as the preferred route for the reaction, these alternative structures highlight the complexity of the overall chemical landscape and the versatility of the V aminotriphenolate catalytic system.

◼ CONCLUSIONS

Our current mechanistic proposal is in good agreement with experimental results regarding the catalytic activity of the eight

relative barrier of only 9.2 kcal·mol^{-1}, a clear improvement over the mechanism in absence of the LB. While S−O bond formation is slightly hindered in comparison with the original manifold, becoming the rate-determining step at 12.0 kcal·mol^{-1}, the facilitation of the proton transfer prevails, and the
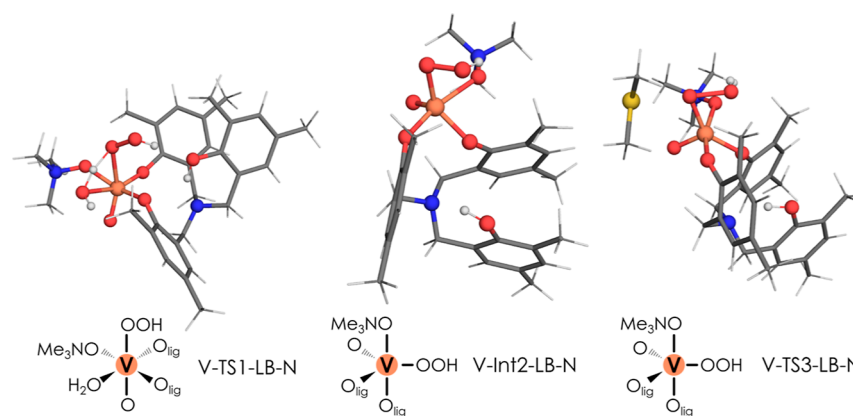
Figure 9. Selected tridimensional structures for V-mediated sulfoxidation in the presence of N-oxide, including proton transfer TS (V-TS1-LB-N), hydroperoxo intermediate (V-Int2-LB-N), and sulfoxidation TS (V-TS3-LB-N). The immediate coordination environment of V(V) is represented schematically next to the corresponding label.
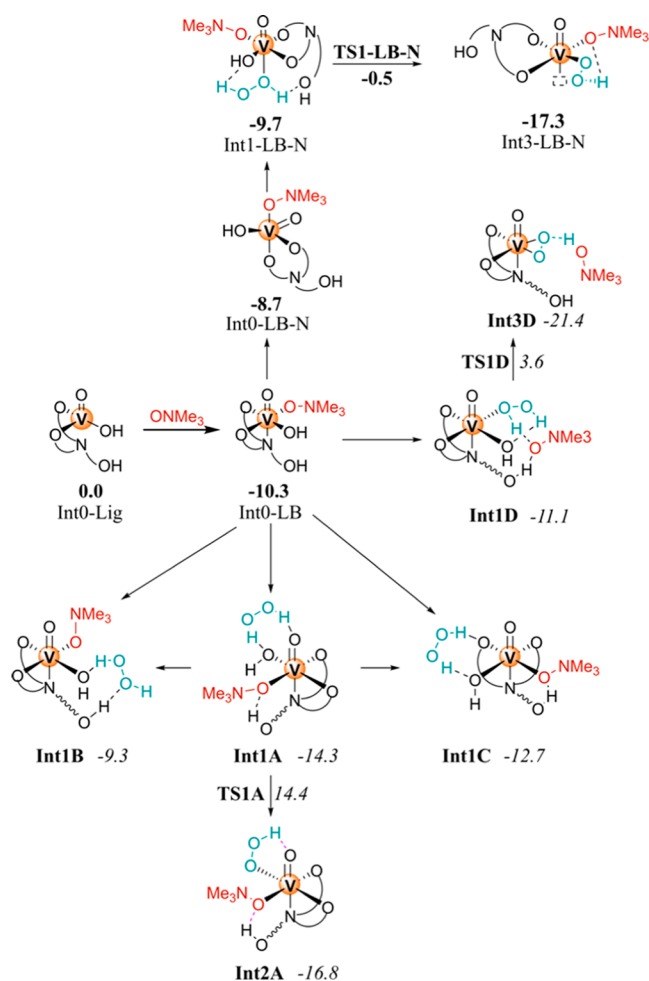

Figure 10. Alternative Int0-Lig + HOOH + ONMe3 coordination complexes. Gibbs free energies including Martin entropic corrections, in kcal·mol^{-1}. Vanadium geometries are specified as oct (octahedral), tbp (trigonal bipyramid), and tet (tetrahedral). Chelated peroxo groups are assumed to occupy a single vacant.

very similar reactivities that are quite different from their lighter group partners (Ti, V). While for group 4 the differences in reactivity come mainly from the differences in ionic radii, group 5 shows a deeper mechanistic shift: the unique substitution pattern of the vanadium complex (with an oxo moiety absent from Nb or Ta) and the basicity of the aminotriphenolate ligand enable the system to maintain the oxo group by partially protonating the ligand. From there, a synergistic effect between the fluxionality of vanadium and the flexibility of the ligand enables the metal to adapt its coordination number across the catalytic cycle, depending on the number of additional ligands that need to be coordinated. Moreover, these synergies do also explain the boost in catalytic activity undergone by the V complex in the presence of an N-oxide which inhibits most of the other metals, as the adaption of the coordination sphere gives room for the oxide to coordinate without blocking other positions.

■ ASSOCIATED CONTENT

Data Availability Statement

All DFT calculations are available as a data set collection in the ioChem-BD repository and can be accessed at https://doi.org/10.19061/iochem-bd-1-302.

Ⓢ Supporting Information

The Supporting Information is available free of charge at https://pubs.acs.org/doi/10.1021/acsomega.4c04831.

> Synthesis and characterization details, kinetic experiments and traces, and calculations (PDF)

■ AUTHOR INFORMATION

Corresponding Authors

Cristiano Zonta — *Dipartimento di Scienze Chimiche, Università degli Studi di Padova, 35131 Padova, Italy; Consorzio Interuniversitario reattività e Catalisi (CIRCC)—Padova UdR, 35131 Padova, Italy;* ⓞ orcid.org/0000-0003-1749-7482; Email: cristiano.zonta@unipd.it

Carles Bo — *Institute of Chemical Research of Catalonia (ICIQ), Barcelona Institute of Science & Technology (BIST), 43007 Tarragona, Spain; Departament de Química Física i Inorgànica, Universitat Rovira i Virgili (URV), 43007 Tarragona, Spain;* ⓞ orcid.org/0000-0001-9581-2922; Email: cbo@iciq.cat

d^0 metal aminotriphenolate complexes studied. Across periods, there is a clear decrease in catalytic performance with increasing charge of the central ion: group 4 (+4) ≫ group 5 (+5) ≫ group 6 (+6). Along the groups, the heavier metals from the fifth and sixth periods (Zr/Hf, Nb/Ta, Mo/W) show

Giulia Licini − *Dipartimento di Scienze Chimiche, Università degli Studi di Padova, 35131 Padova, Italy; Consorzio Interuniversitario reattività e Catalisi (CIRCC)—Padova UdR, 35131 Padova, Italy;* ⦿ orcid.org/0000-0001-8304-0443; Email: giulia.licini@unipd.it

Authors

Diego Garay-Ruiz − *Institute of Chemical Research of Catalonia (ICIQ), Barcelona Institute of Science & Technology (BIST), 43007 Tarragona, Spain;* ⦿ orcid.org/0000-0003-0744-0562

Silvia Lovat − *Dipartimento di Scienze Chimiche, Università degli Studi di Padova, 35131 Padova, Italy*

Fátima Sanz Azcona − *Dipartimento di Scienze Chimiche, Università degli Studi di Padova, 35131 Padova, Italy; Consorzio Interuniversitario reattività e Catalisi (CIRCC)— Padova UdR, 35131 Padova, Italy*

Joan González-Fabra − *Institute of Chemical Research of Catalonia (ICIQ), Barcelona Institute of Science & Technology (BIST), 43007 Tarragona, Spain*

Complete contact information is available at:
https://pubs.acs.org/10.1021/acsomega.4c04831

■ REFERENCES

(1) Limberg, C.; Meyer, F. Organometallic Oxidation Catalysis. In *Topics in Organometallic Chemistry*; Springer-Verlag: Berlin, 2007.

(2) Backvall, J.-E. *Modern Oxidation Methods*; Wiley VCH: New York, 2004.

(3) Caron, S.; Dugger, R. W.; Ruggeri, S. G.; Ragan, J. A.; Ripin, D. H. B. Large-Scale Oxidations in the Pharmaceutical Industry. *Chem. Rev.* **2006**, *106* (7), 2943−2989.

(4) Vicens, L.; Olivo, G.; Costas, M. Rational Design of Bioinspired Catalysts for Selective Oxidations. *ACS Catal.* **2020**, *10* (15), 8611−8631.

(5) Yoon, C. W.; Hirsekorn, K. F.; Neidig, M. L.; Yang, X.; Tilley, T. D. Mechanism of the Decomposition of Aqueous Hydrogen Peroxide over Heterogeneous TiSBA15 and TS-1 Selective Oxidation Catalysts: Insights from Spectroscopic and Density Functional Theory Studies. *ACS Catal.* **2011**, *1* (12), 1665−1678.

(6) Maksimchuk, N. V.; Puiggalí-Jou, J.; Zalomaeva, O. V.; Larionov, K. P.; Evtushok, V. Y.; Soshnikov, I. E.; Solé-Daura, A.; Kholdeeva, O. A.; Poblet, J. M.; Carbó, J. J. Resolving the Mechanism for H_2O_2 Decomposition over Zr(IV)-Substituted Lindqvist Tungstate: Evidence of Singlet Oxygen Intermediacy. *ACS Catal.* **2023**, *13* (15), 10324−10339.

(7) Bach, R. D.; Schlegel, H. B. Mechanism of Orbital Interactions in the Sharpless Epoxidation with Ti(IV) Peroxides: A DFT Study. *J. Phys. Chem. A* **2021**, *125* (49), 10541−10556.

(8) Conte, V.; Coletti, A.; Floris, B.; Licini, G.; Zonta, C. Mechanistic Aspects of Vanadium Catalysed Oxidations with Peroxides. *Coord. Chem. Rev.* **2011**, *255*, 2165−2177.

(9) Mimoun, H. Do metal peroxides as homolytic and heterolytic oxidative reagents. Mechanism of the halcon epoxidation process. *Catal. Today* **1987**, *1* (3), 281−295.

(10) Kirihara, M.; Yamamoto, J.; Noguchi, T.; Itou, A.; Naito, S.; Hirai, Y. Tantalum(V) or niobium(V) catalyzed oxidation of sulfides with 30% hydrogen peroxide. *Tetrahedron* **2009**, *65* (50), 10477−10484.

(11) Krohn, K.; Vinke, I.; Adam, H. Transition-Metal Catalyzed Oxidations. 7. Zirconium-Catalyzed Oxidation of Primary and Secondary Alcohols with Hydroperoxides. *J. Org. Chem.* **1996**, *61* (4), 1467−1472.

(12) Bonchio, M.; Licini, G.; Di Furia, F.; Mantovani, S.; Modena, G.; Nugent, W. A. The First Chiral Zirconium(IV) Catalyst for Highly Stereoselective Sulfoxidation. *J. Org. Chem.* **1999**, *64* (4), 1326−1330.

(13) Watanabe, A.; Uchida, T.; Irie, R.; Katsuki, T. Zr[Bis-(Salicylidene)Ethylenediaminato]-Mediated Baeyer-Villiger Oxidation: Stereospecific Synthesis of Abnormal and Normal Lactones. *Proc. Natl. Acad. Sci. U.S.A.* **2004**, *101*, 5737−5742.

(14) Egami, H.; Katsuki, T. Nb(Salan)-Catalyzed Asymmetric Epoxidation of Allylic Alcohols with Hydrogen Peroxide. *Angew. Chem., Int. Ed.* **2008**, *47* (28), 5171−5174.

(15) Antonova, N. S.; Carbó, J. J.; Kortz, U.; Kholdeeva, O. A.; Poblet, J. M. Mechanistic Insights into Alkene Epoxidation with H_2O_2 by Ti- and Other TM-Containing Polyoxometalates: Role of the Metal Nature and Coordination Environment. *J. Am. Chem. Soc.* **2010**, *132* (21), 7488−7497.

(16) Maksimchuk, N. V.; Ivanchikova, I. D.; Maksimov, G. M.; Eltsov, I. V.; Evtushok, V. Y.; Kholdeeva, O. A.; Lebbie, D.; Errington, R. J.; Solé-Daura, A.; Poblet, J. M.; Carbó, J. J. Why Does Nb(V) Show Higher Heterolytic Pathway Selectivity Than Ti(IV) in Epoxidation with H_2O_2? Answers from Model Studies on Nb- and Ti-Substituted Lindqvist Tungstates. *ACS Catal.* **2019**, *9* (7), 6262−6275.

(17) Maksimchuk, N. V.; Evtushok, V. Y.; Zalomaeva, O. V.; Maksimov, G. M.; Ivanchikova, I. D.; Chesalov, Y. A.; Eltsov, I. V.; Abramov, P. A.; Glazneva, T. S.; Yanshole, V. V.; Kholdeeva, O. A.; Errington, R. J.; Solé-Daura, A.; Poblet, J. M.; Carbó, J. J. Activation of H_2O_2 over Zr(IV). Insights from Model Studies on Zr-Monosubstituted Lindqvist Tungstates. *ACS Catal.* **2021**, *11* (16), 10589−10603.

(18) Maksimchuk, N. V.; Evtushok, V. Y.; Zalomaeva, O. V.; Maksimov, G. M.; Ivanchikova, I. D.; Chesalov, Y. A.; Eltsov, I. V.; Abramov, P. A.; Glazneva, T. S.; Yanshole, V. V.; Kholdeeva, O. A.; Errington, R. J.; Solé-Daura, A.; Poblet, J. M.; Carbó, J. J. Activation of H_2O_2 over Zr(IV). Insights from Model Studies on Zr-Monosubstituted Lindqvist Tungstates. *ACS Catal.* **2021**, *11* (16), 10589−10603.

(19) Gall, R. D.; Faraj, M.; Hill, C. L. Role of Water in Polyoxometalate-Catalyzed Oxidations in Nonaqueous Media.

Scope, Kinetics, and Mechanism of Oxidation of Thioether Mustard (HD) Analogs by Tert-Butyl Hydroperoxide Catalyzed by H5PV2Mo10O40. *Inorg. Chem.* **1994**, *33* (22), 5015–5021.

(20) Di Valentin, C.; Gisdakis, P.; Yudanov, I. V.; Rösch, N. Olefin Epoxidation by Peroxo Complexes of Cr, Mo, and W. A Comparative Density Functional Study. *J. Org. Chem.* **2000**, *65* (10), 2996–3004.

(21) Licini, G.; Mba, M.; Zonta, C. Amine Triphenolate Complexes: Synthesis, Structure and Catalytic Activity. *Dalton Trans.* **2009**, No. 27, 5265–5277.

(22) Lovat, S.; Mba, M. C. L.; Abbenhuis, H.; Vogt, D.; Zonta, C.; Licini, G. Role of Intermolecular Interactions in Oxygen Transfer Catalyzed by Silsesquioxane Trisilanolate Vanadium(V). *Inorg. Chem.* **2009**, *48* (11), 4724–4728.

(23) Prins, L. J.; Blázquez, M. M.; Kolarović, A.; Licini, G. Effective Synthesis of Ortho-Substituted Triphenol Amines via Reductive Amination. *Tetrahedron Lett.* **2006**, *47* (16), 2735–2738.

(24) Mba, M.; Prins, L. J.; Zonta, C.; Cametti, M.; Valkonen, A.; Rissanen, K.; Licini, G. Ti(Iv)-Amino Triphenolate Complexes as Effective Catalysts for Sulfoxidation. *Dalton Trans.* **2010**, *39* (31), 7384–7392.

(25) Mba, M.; Pontini, M.; Lovat, S.; Zonta, C.; Bernardinelli, G.; Kündig, P. E.; Licini, G. C3 Vanadium(V) Amine Triphenolate Complexes: Vanadium Haloperoxidase Structural and Functional Models. *Inorg. Chem.* **2008**, *47* (19), 8616–8618.

(26) Laurén, E.; Kivelä, H.; Hänninen, M.; Lehtonen, A. Oxidomolybdenum(VI) Complexes with Atrane-Type [O3N] Ligands. *Polyhedron* **2009**, *28* (18), 4051–4055.

(27) Romano, F.; Linden, A.; Mba, M.; Zonta, C.; Licini, G. Molybdenum(VI) Amino Triphenolate Complexes as Catalysts for Sulfoxidation, Epoxidation and Haloperoxidation. *Adv. Synth. Catal.* **2010**, *352* (17), 2937–2942.

(28) Badetti, E.; Bonetto, A.; Romano, F.; Marchiò, L.; Zonta, C.; Licini, G. Synthesis, Characterization and Catalytic Activity of a Tungsten(VI) Amino Triphenolate Complex. *Catal. Lett.* **2017**, *147* (9), 2313–2318.

(29) Jeong, N. C.; Lee, J. S.; Tae, E. L.; Lee, Y. J.; Yoon, K. B. Acidity Scale for Metal Oxides and Sanderson's Electronegativities of Lanthanide Elements. *Angew. Chem., Int. Ed.* **2008**, *47* (52), 10128–10132.

(30) Sanderson, R. T. Electronegativity and bonding of transitional elements. *Inorg. Chem.* **1986**, *25* (19), 3518–3522.

(31) Sanderson, R. T. Electronegativity and Bond Energy. *J. Am. Chem. Soc.* **1983**, *105*, 2259–2261.

(32) Sanderson, R. *Chemical Bonds and Bonds Energy*; Academic Press: New York, 1976.

(33) Sanderson, R. T. An Interpretation of Bond Lengths and a Classification of Bonds. *Science* **1951**, *114* (2973), 670–672.

(34) Perdew, J. P. Density-Functional Approximation for the Correlation Energy of the Inhomogeneous Electron Gas. *Phys. Rev. B* **1986**, *33*, 8822–8824.

(35) Selloni, A.; Carnevali, P.; Tosatti, E.; Chen, C. D. Erratum: Voltage-Dependent Scanning-Tunneling Microscopy of a Crystal Surface: Graphite. *Phys. Rev. B* **1986**, *34*, 7406.

(36) Grimme, S.; Antony, J.; Ehrlich, S.; Krieg, H. A Consistent and Accurate Ab Initio Parametrization of Density Functional Dispersion Correction (DFT-D) for the 94 Elements H-Pu. *J. Chem. Phys.* **2010**, *132* (15), 154104.

(37) Lenthe, E. V.; Baerends, E. J.; Snijders, J. G. Relativistic Regular Two-Component Hamiltonians. *J. Chem. Phys.* **1993**, *99* (6), 4597–4610.

(38) Van Lenthe, E.; Baerends, E. J.; Snijders, J. G. Relativistic Total Energy Using Regular Approximations. *J. Chem. Phys.* **1994**, *101* (11), 9783–9792.

(39) Van Lenthe, E.; Ehlers, A.; Baerends, E.-J. Geometry Optimizations in the Zero Order Regular Approximation for Relativistic Effects. *J. Chem. Phys.* **1999**, *110* (18), 8943–8953.

(40) Pye, C. C.; Ziegler, T. An Implementation of the Conductor-like Screening Model of Solvation within the Amsterdam Density Functional Package. Theoretical Chemistry Accounts: Theory,

Computation, and Modelling. *Theor. Chim. Acta* **1999**, *101* (6), 396–408.

(41) Baerends, E. J.; Ziegler, T.; Atkins, A. J.; Autschbach, J.; Baseggio, O.; Bashford, D.; Bérces, A.; Bickelhaupt, F. M.; Bo, C.; Boerritger, P. M.; Cavallo, L.; Daul, C.; Chong, D. P.; Chulhai, D. V.; Deng, L.; Dickson, R. M.; Dieterich, J. M.; Ellis, D. E.; van Faassen, M.; Fan, L.; Fischer, T. H.; Guerra, C. F.; Franchini, M.; Ghysels, A.; Giammona, A.; van Gisbergen, S. J. A.; Goez, A.; Götz, A. W.; Groeneveld, J. A.; Gritsenko, O. V.; Gruning, M.; Gusarov, S.; Harris, F. E.; van den Hoek, P.; Hu, Z.; Jacob, C. R.; Jacobsen, H.; Jensen, L.; Joburet, L.; Kaminski, J. W.; van Kessel, G.; Konig, C.; Kootstra, F.; Kovalenko, A.; Krykunov, M. V.; van Lenthe, E.; McCormack, D. A.; Michalak, A.; Mitoraj, M.; Morton, S. M.; Neugebauer, J.; Nicu, V. P.; Noodleman, L.; Osinga, V. P.; Patchkovskii, S.; Pavanello, M.; Peeples, C. A.; Philipsen, P. H. T.; Post, D.; Pye, C. C.; Ramanantoanina, H.; Ramos, P.; Ravenek, W.; Rodríguez, J. I.; Ros, P.; Rüger, R.; Schipper, P. R. T.; Schluns, D.; van Schoot, H.; Schreckenbach, G.; Seldenthuis, J. S.; Seth, M.; Snijders, J. G.; Solà, M.; Stener, M.; Swart, M.; Swerhone, D.; te Velde, G.; Vernooijs, P.; Versluis, L.; Visscher, L.; Visser, O.; Wang, F.; Wesolowski, T. A.; van Wezenbeek, E. M.; Wiesenekker, G.; Wolff, S. K.; Woo, T. K.; Yakovlev, A. L. *ADF2016, SCM, Theoretical Chemistry*; Vrije Universiteit: Amsterdam, The Netherlands, 2018.

(42) Martin, R. L.; Hay, P. J.; Pratt, L. R. Hydrolysis of Ferric Ion in Water and Conformational Equilibrium. *J. Phys. Chem. A* **1998**, *102*, 3565–3573.

(43) Clerici, M. G. Oxidation of saturated hydrocarbons with hydrogen peroxide, catalysed by titanium silicalite. *Appl. Catal.* **1991**, *68* (1), 249–261.

(44) Tantanak, D.; Vincent, M. A.; Hillier, I. H. Elucidation of the Mechanism of Alkene Epoxidation by Hydrogen Peroxide Catalysed by Titanosilicates: A Computational Study. *Chem. Commun.* **1998**, No. 9, 1031–1032.

(45) Yudanov, I. V.; Gisdakis, P.; Di Valentin, C.; Rösch, N. Activity of Peroxo and Hydroperoxo Complexes of TiIV in Olefin Epoxidation: A Density Functional Model Study of Energetics and Mechanism. *Eur. J. Inorg. Chem.* **1999**, *1999* (12), 2135–2145.

(46) Rösch, N.; Di Valentin, C.; Yudanov, I. V. Mechanism of Olefin Epoxidation by Transition Metal Peroxo Compounds. In *Computational Modeling of Homogeneous Catalysis*; Maseras, F., Lledós, A., Eds.; Springer US: Boston, MA, 2002; Vol. 25, pp 289–324..

(47) To, J.; Sokol, A. A.; French, S. A.; Catlow, C. R. A. Hybrid QM/MM Investigations into the Structure and Properties of Oxygen-Donating Species in TS-1. *J. Phys. Chem. C* **2008**, *112* (18), 7173–7185.

(48) Solé-Daura, A.; Zhang, T.; Fouilloux, H.; Robert, C.; Thomas, C. M.; Chamoreau, L.-M.; Carbó, J. J.; Proust, A.; Guillemot, G.; Poblet, J. M. Catalyst Design for Alkene Epoxidation by Molecular Analogues of Heterogeneous Titanium-Silicalite Catalysts. *ACS Catal.* **2020**, *10* (8), 4737–4750.

(49) Garay-Ruiz, D.; Zonta, C.; Lovat, S.; González-Fabra, J.; Bo, C.; Licini, G. Elucidating Sulfide Activation Mode in Metal-Catalyzed Sulfoxidation Reactivity. *Inorg. Chem.* **2022**, *61* (10), 4494–4501.

(50) Gall, R. D.; Faraj, M.; Hill, C. L. Role of Water in Polyoxometalate-Catalyzed Oxidations in Nonaqueous Media. Scope, Kinetics, and Mechanism of Oxidation of Thioether Mustard (HD) Analogs by tert-Butyl Hydroperoxide Catalyzed by H5PV2Mo10O40. *Inorg. Chem.* **1994**, *33*, 5015–5021.